Electronic Supplementary Material (ESI) for Nanoscale Advances.
This journal is © The Royal Society of Chemistry 2022

SUPPORTING INFORMATION TO:

Flexible and transparent electrodes imprinted from metal nanostructures: morphology and opto-electronic performance

Lukas F. Engel,[†] Lola González-García,[*,†] and Tobias Kraus[*,†,‡]

†*INM — Leibniz Institute for New Materials, Campus D2 2, 66123 Saarbrücken, Germany*

‡*Colloid and Interface Chemistry, Saarland University, Campus D2 2, 66123 Saarbrücken, Germany*

E-mail: lola.gonzalez-garcia@leibniz-inm.de; tobias.kraus@leibniz-inm.de

1 Nanoimprinting method

The nano-objects were assembled into the desired structure using direct nanoimprinting. We illustrate the method using the example of AuNW and a hexagonally patterned stamp because spherical particles and other stamp patterns do not change the procedure. A patterned PDMS stamp (1) was attached to a steel cylinder and rolled over a substrate that carried a sessile droplet of the AuNW ink (2). The ink is confined by the stamp's cavities, the solvent permeates the PDMS, particle concentration slowly increases, the AuNW self-assemble into larger bundles (3) and finally percolate. The resulting structures (4) closely follow the stamp features.[1]

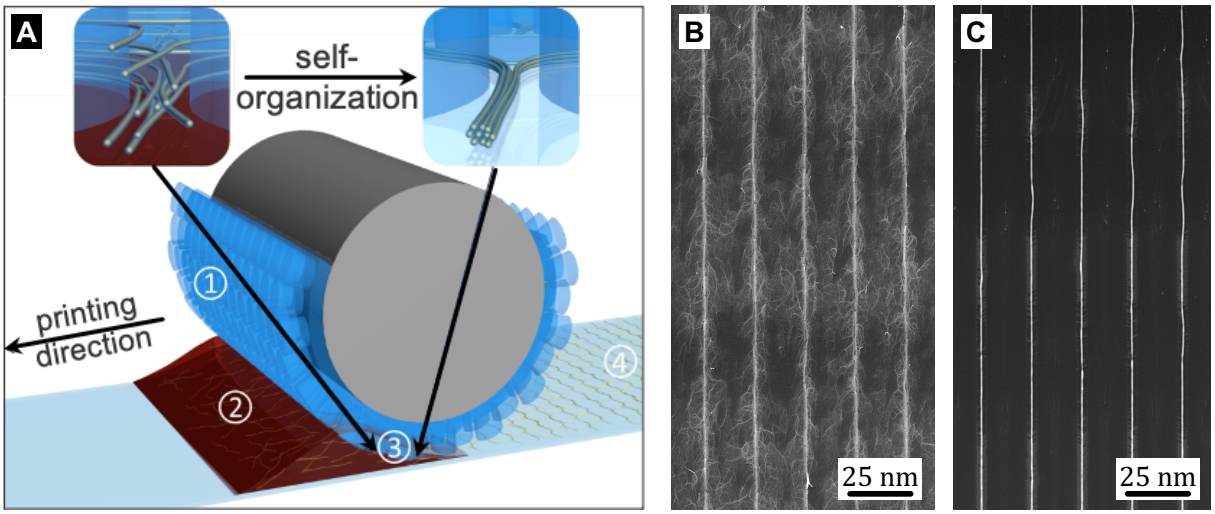

Figure S1: **A**: Nanoimprinting with (1) a hexagonally patterned PDMS stamp attached to a steel cylinder, (2) the AuNW-based ink confined between PET substrate and stamp, (3) AuNW self-assembly upon solvent permeation through the stamp, and (4) the resulting Au grid. Figure adapted from Maurer et al..[1] **B**: SEM micrograph of a AuNW-based line grid electrode imprinted at 6 mg/mL on Si, after plasma sintering. **C**: SEM micrograph of a AuNP-based line grid electrode imprinted at 30 mg/mL on Si, after plasma sintering.

The imprinting stamps had an area of 3.5 cm x 8 cm, of which 3.5 cm x 7 cm were patterned. The flat 3.5 cm x 0.5 cm at either end of the stamp served as run-in and run-out areas during imprinting. The stamp pattern consisted of parallel, line-like channels with a pitch $p \approx 19.5\,\mu m$, a channel width $w_c \approx 1.6\,\mu m$ and a channel depth $d_c \approx 4.2\,\mu m$.

2 Fitting the opto-electronic trade-off

Sheet resistance R_{sh} was determined as the resistance R of a square electrode section of edge length $l = 15\,000\,\mu m$, contacted with Ag paste and miniature crocodile clamps in two-point-probe configuration. Such a sub-area comprised 750 conductive lines and had an anisotropic sheet resistance of

$$R_{sh}^{-1} = R^{-1} = G = \sigma_{shell} \cdot \frac{750 \cdot A_{shell}}{l}, \tag{S1}$$

measured parallel to the lines, where G is the overall conductance of 750 parallel lines.

To reduce the weight of the R_{sh} data points at the lowest concentration c_{Au} (which were off-the-charts) during fitting of the trade-off between sheet resistance and optical transmittance, we thus used the relation above to fit $R_{sh}^{-1} = G$ vs. $\overline{T}_{400-800\,nm}$ rather than R_{sh} vs. $\overline{T}_{400-800\,nm}$. The fits in Fig. S2B are therefore the inverse of the linear fits in Fig. S2A.

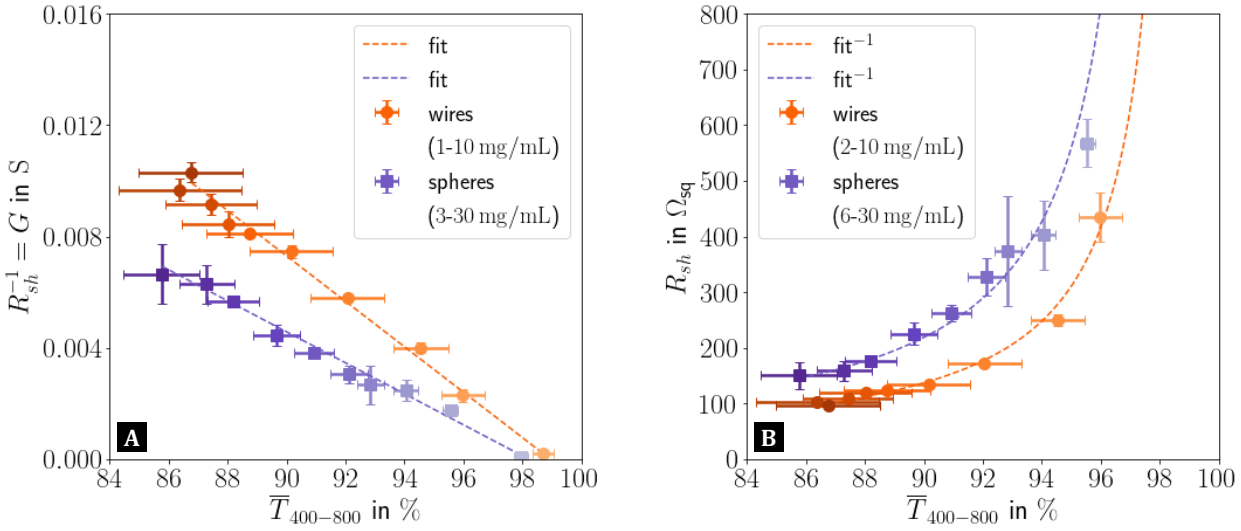

Figure S2: Trade-off between **(A)** conductance $G = R_{sh}^{-1}$ and optical transmittance $\overline{T}_{400-800}$ as well as **(B)** between sheet resistance R_{sh} and optical transmittance $\overline{T}_{400-800}$ for both AuNW and AuNP based electrodes directly after plasma sintering. Data points for $c_{Au}^{wires} = 1\,mg/mL$ and $c_{Au}^{spheres} = 3\,mg/mL$ have been omitted in B due to off-the-chart high R_{sh} (up to two orders of magnitude higher). | All graphs show average values from three measurements each and the belonging standard deviation. The colour gradient reflects the concentration gradient, with light colours representing the lowest and dark colours the highest concentration.

3 Spherical gold nanoparticle dispersion

SAXS measurements were carried out to determine the average AuNP diameter d_{sp} and to study the AuNP agglomeration state over the entire concentration range used for imprinting.

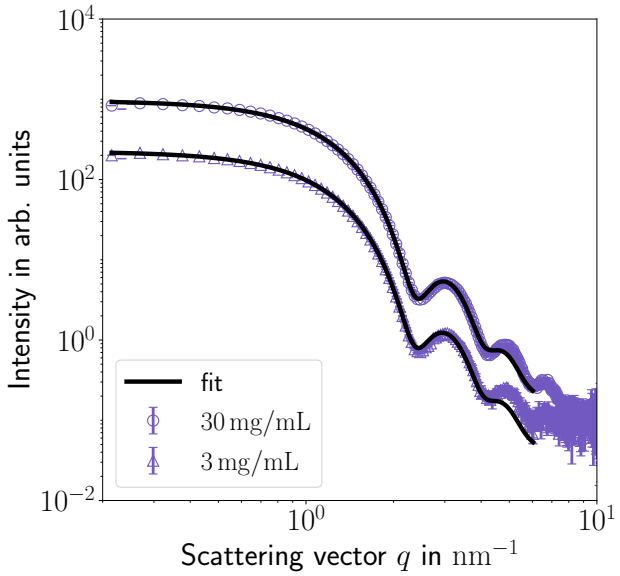

Figure S3: Radially integrated and fitted SAXS curves of the AuNP used for nanoimprinting at both the lowest (3 mg/mL) and the highest concentration (30 mg/mL). No agglomeration peaks are visible. The core size is $d_{sp} = 3.7\,\mathrm{nm} \pm 10\,\%$.

4 Morphology of plasma-sintered electrodes

4.1 Electrode topography

CLSM was used to characterize the electrode topography and to derive the conductor geometry thereof. Each topography map consisted of 1240 equidistant height traces across eight parallel conductor segments.

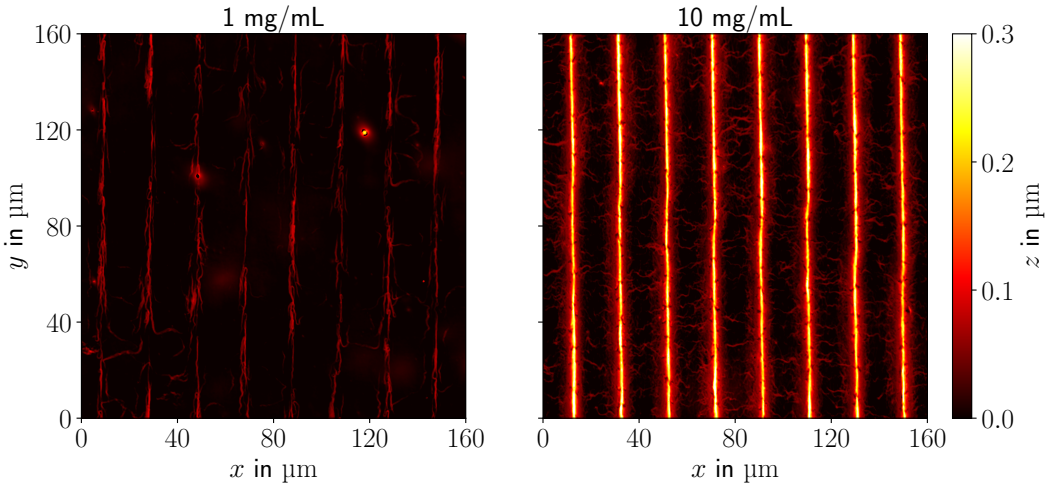

Figure S4: Exemplary CLSM topography maps of AuNW-based electrode sections after plasma sintering for the lowest (1 mg/mL) and the highest (10 mg/mL) concentration c_{Au}.

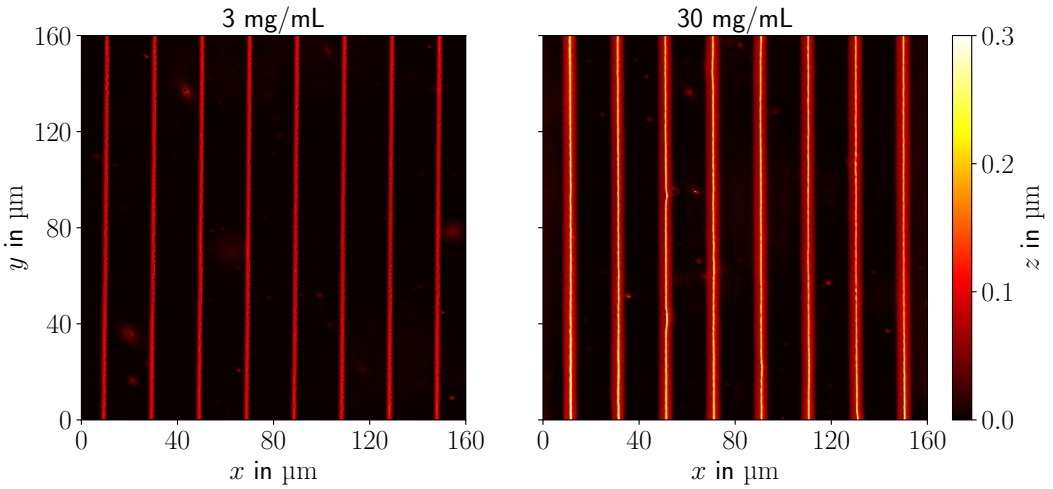

Figure S5: Exemplary CLSM topography maps of AuNP-based electrode sections after plasma sintering for the lowest (3 mg/mL) and the highest (30 mg/mL) concentration c_{Au}.

4.2 Determining the average conductor shell thickness

To determine the average conductor shell thickness t_{shell}, TEM images were taken after plasma-sintering from FIB cross-sections which had been thinned out strongly to reveal the true shell thickness (Fig. S6). In particular the such revealed shell morphology of the AuNW-based electrodes was compared with SEM surface images to rule out the possibility that the observed holes (blue arrows) were due to the FIB milling. The shell thicknesses (in nm) were measured in ten approximately equidistant locations each and were then averaged.

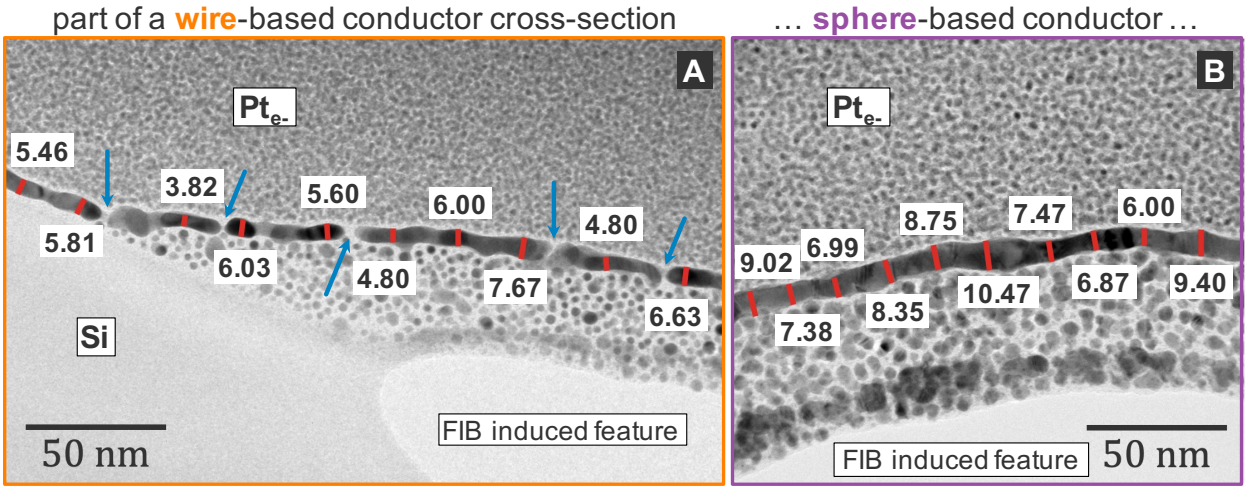

Figure S6: **(A)** shows a part of a AuNW-based conductor cross-section (6 mg/mL) with $t_{shell} = 5.66 \pm 1.06$ nm and **(B)** depicts a part of a AuNP-based conductor cross-section (30 mg/mL) with $t_{shell} = 8.07 \pm 1.36$ nm. So both shell thicknesses were well below the electron mean free path of bulk Au which amounts to $\lambda_{Au} \approx 37.7$ nm at room temperature.[2]

4.3 Defects in sphere-based conductors after plasma sintering

Subtle defects occurring at concentrations close to the percolation threshold could be revealed with SEM (Fig. S7).

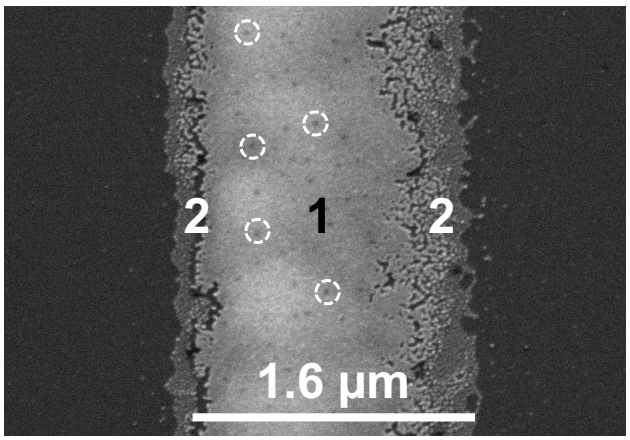

Figure S7: Exemplary post-plasma electrode conductor surface morphology (high-magnification SEM top view) on Si substrate at the lowest concentration c_{Au} (3 mg/mL) used for nanoimprinting with AuNP. (1) designates the conducting part and (2) the non-conducting edges. The dashed circles indicate pores exemplary. | Note that the scale bar has the width w_c of the stamp's channel.

Severe defects could be detected with CLSM. They were less common and thus harder to find, but were present even at high c_{Au} (Fig. S8).

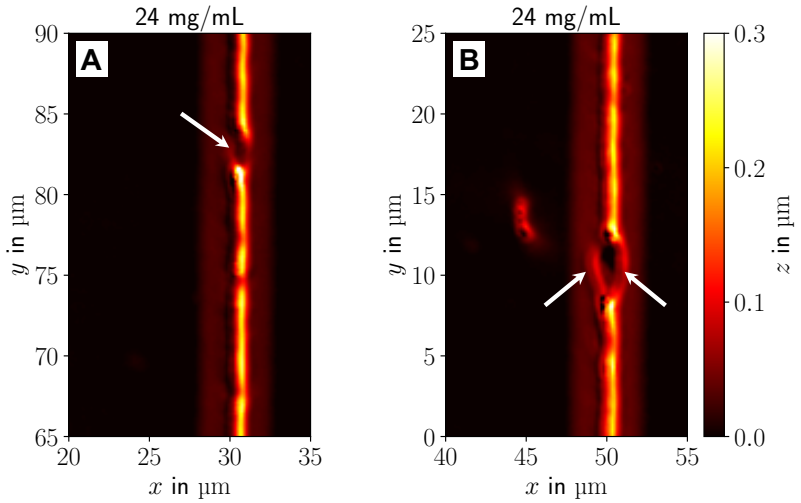

Figure S8: **A:** Fully interrupted conductor (white arrow). **B:** Interrupted conductor with bypasses on either side (white arrows) effectively resulting in a line tapering.

4.4 Post-plasma conductor aspect ratios

The conductor aspect ratios illustrate how conductor width w and maximum conductor height h_{max} develop in relation to each other with increasing concentration c_{Au} (Fig. S9).

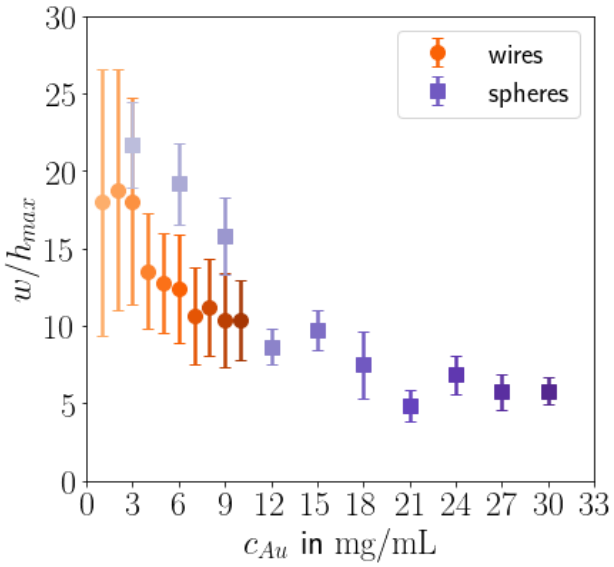

Figure S9: Evolution of the conductor aspect ratios with concentration. The graph shows average values and the belonging standard deviation. The colour gradient reflects the concentration gradient, with light colours representing the lowest and dark colours the highest concentration.

5 Electrode model unit cell: optical transmittance

An electrode unit cell was used to model the electrodes' optical transmittance under the assumption of completely opaque conductors (Fig. S10).

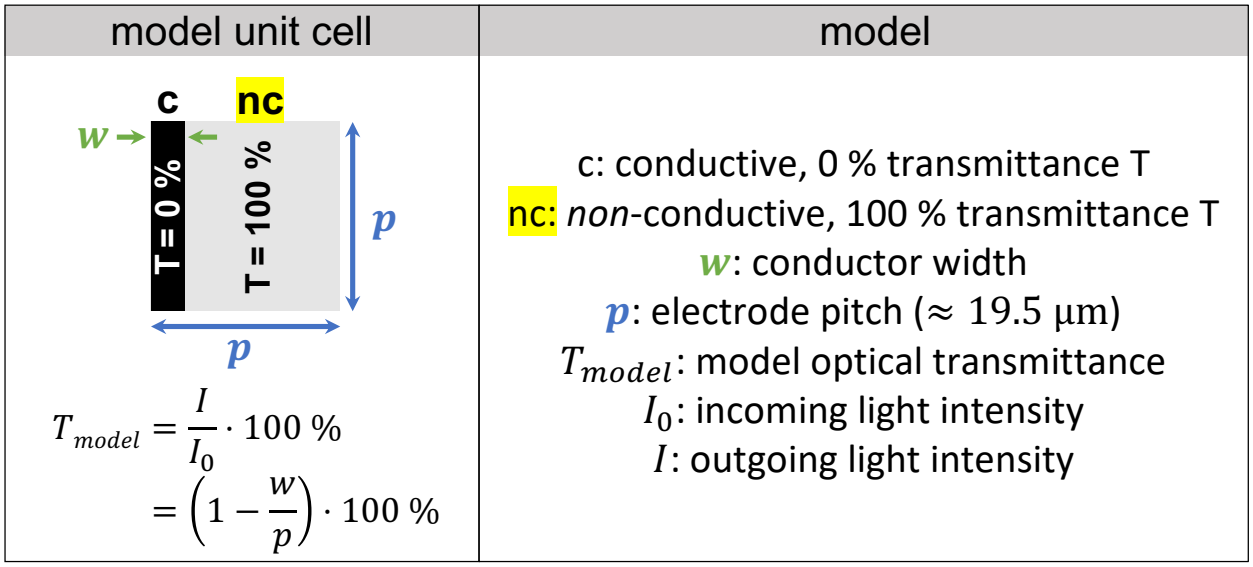

Figure S10: Scheme of the electrode model unit cell.

References

(1) Maurer, J. H. M.; González-García, L.; Backes, I. K.; Reiser, B.; Schlossberg, S. M.; Kraus, T. Direct Nanoimprinting of a Colloidal Self-Organizing Nanowire Ink for Flexible, Transparent Electrodes. *Advanced Materials Technologies* **2017**, *2*, 1700034.

(2) Gall, D. Electron mean free path in elemental metals. *Journal of Applied Physics* **2016**, *119*, 085101.